JOURNAL OF CATALYSIS 137, 357–367 (1992)

Formation of Small Pt–Ir Bimetallic Clusters in NaY Zeolite Probed with ^{129}Xe NMR Spectroscopy and Ethane Hydrogenolysis

O BONG YANG,* SEONG IHL WOO,*,[1] AND RYONG RYOO†

*Department of Chemical Engineering, Korea Advanced Institute of Science and Technology, P.O. Box 150, Cheongryang, Seoul, Korea; and †Department of Chemistry, Korea Advanced Institute of Science and Technology Taeduk Science Town, Taejon, 305-701 Korea

Received June 18, 1991; revised April 8, 1992

Very small (about 1 nm) and homogeneous Pt–Ir bimetallic clusters were formed in the zeolite supercage by calcining NaY co-ion-exchanged with $Pt(NH_3)_4^{2+}$ and $Ir(NH_3)_5Cl^{2+}$ at room temperature and subsequent reduction treatment with H_2 at 573 K. These bimetallic clusters were characterized by hydrogen and xenon adsorption, X-ray differaction (XRD), ^{129}Xe NMR spectroscopy, and ethane hydrogenolysis reaction. Pt–Ir bimetallic clusters showed specific characteristics different from those of Pt and Ir monometallic clusters and physical mixtures of corresponding monometallic clusters. The chemical shifts of Pt–Ir bimetallic clusters in ^{129}Xe NMR and their catalytic activities in ethane hydrogenolysis were lower than those of the corresponding physical mixtures of Pt and Ir monometallic clusters. The activation energies of Pt–Ir bimetallic clusters in ethane hydrogenolysis were smaller than those of monometallic Pt and Ir clusters. The turnover frequencies (TOFs) of bimetallic clusters in ethane hydrogenolysis are widely different from those of monometallic clusters.

INTRODUCTION

Bimetallic catalysts are widely used in the chemical and petroleum industries. During the last decade such bimetallic catalysts as Pt–Ir (*1–4*), Pt–Re (*5–8*), and Pt–Sn (*9, 10*) have replaced the monometallic Pt (*11, 12*) catalyst in the naphtha reforming process. It was reported that bimetallic catalysts often possess specific characteristics different from those of monometallic clusters and the physical mixture of corresponding monometallic clusters (*1–10*). However, a satisfactory understanding of these special characters of bimetallic catalysts is not yet to be found.

In recent years, the effect of the cluster size on the chemisorptive and catalytic properties has been investigated, which may build a bridge between homogeneous and heterogeneous catalysis. The clusters of the diameter less than 1.3 nm were prepared inside the supercage of NaY (*13, 14*). Elliott and Lunsford (*15*) studied Ru–Cu bimetallic clusters entrapped in NaY. Tebassi *et al.* (*16*) characterized Pt–Cu, Ru–Cu, and Rh–Cu in NaY zeolite. Pt–Mo in Y Zeolites was also studied by Tri *et al.* (*17*). Pt–Re in NaHY and Pt–Cu in NaY have been studied by Sachtler and co-workers (18, 19).

A number of physical and chemical techniques are available for the characterization of bimetallic clusters. However, most of these physical probe have some limitations. Although Gronsky and co-workers (*20*) investigated the visibility of a 13-atom Pt cluster in the zeolite channel with high-resolution electron microscopy (HREM), it is still difficult to characterize very small clusters with the electron microscopic method (*21*). Extended X-ray absorption fine structure (EXAFS) (22–24) studies are very useful for the study of bimetallic clusters. However, it is not applicable to all the pairs of metal elements. For highly diluted Pt–Re clusters EXAFS cannot be utilized (*25*). Mössbauer

[1] To whom correspondence should be addressed.

0021-9517/92 $5.00

spectroscopy has been used in the characterization of paramagnetic bimetallic catalysts (*26, 27*). This technique is limited to nuclei which produce Mössbauer signals.

Recently, Fraissard and co-workers (*28–30*) have found that the ^{129}Xe NMR of xenon gas adsorbed on zeolites is a very sensitive probe of local environment inside the zeolite channel (*28–31*). Boudart *et al.* (*32*) and Chmelka *et al.* (*33*) used ^{129}Xe NMR to characterize the small Pt cluster in Y zeolite. The adsorbed xenon atoms can be more or less polarized by rapid collisions with the zeolite wall, other xenon atoms, and other species present inside the zeolite channel, or by the adsorption on the zeolite wall. The magnitude of the polarization is signaled by the chemical shift of ^{129}Xe NMR. The chemical shift of ^{129}Xe NMR can thus become a useful probe to monitor the changes in the chemical state and the number of active species inside the supercage of Y zeolites. However, the species located inside the sodalite cage cannot alter the chemical shift, because a xenon atom of 0.43 nm in diameter cannot enter through the window of a sodalite cage of 0.22 nm in diameter. The change in the chemical shift caused by the active species located on the external surface of the zeolite crystal is also negligible, since the number of collision of xenon with the zeolite wall or active species inside zeolite is much greater than that of xenon collision with the active species located on the external surface. In this way ^{129}Xe NMR provides a useful information about the physicochemical nature of a metallic species within the supercage of zeolite.

Sinfelt and co-workers reported that the bimetallic clusters of Pt and Ir were formed on silica (*20, 24*) and alumina (*26*). Highly dispersed bimetallic clusters of Pt and Ir were produced after calcination in air at 573 K, while the oxidative agglomeration of Ir produced large IrO_2 crystallites above the calcination temperature of 773 K (*20, 24, 26, 34*). Kuijers and Ponec (*35*) reported that a pronounced surface enrichment of Pt was observed in Pt–Ir alloys prepared by evaporating Pt and Ir onto a quartz substrate.

TABLE 1

Chemical Composition of the Samples

Sample	wt% Pt	wt% Ir	Ir/(Pt + Ir)
Pt(4)/NaY	4.0	0.0	0.00
Pt(3)Ir(1)/NaY	3.0	1.0	0.25
Pt(2)Ir(2)/NaY	2.0	2.0	0.50
Pt(1)Ir(3)/NaY	1.0	3.0	0.75
Ir(4)/NaY	0.0	4.0	1.00

Not any works have been known to us for characterization of Pt–Ir bimetallic clusters supported in NaY. The physicochemical characteristics of Pt–Ir bimetallic clusters are varied depending on the size of metal clusters and the kind of support material. Therefore, we prepared highly monodispersed (diameter = 1 nm) monometallic Pt and Ir clusters and a series of Pt–Ir bimetallic clusters supported in NaY. ^{129}Xe NMR spectroscopy, XRD, hydrogen and Xe adsorption, and ethane hydrogenolysis reaction were used to probe the formation of Pt–Ir bimetallic clusters.

EXPERIMENTAL

Preparation of Clusters in NaY

A NaY zeolite of average diameter of 0.7 μm supplied by Strem Chem. Co. was used as a support. Monometallic Pt and Ir clusters in NaY (abbreviated as Pt(x)/NaY and Ir(x)/NaY and x indicates wt%) were prepared by calcining and reducing $Pt(NH_3)_4^{2+}$-exchanged NaY and $Ir(NH_3)_5Cl^{2+}$-exchanged NaY with O_2 and H_2 at 573 K, respectively. Pt–Ir bimetallic clusters in NaY (Pt(x)Ir(x)/NaY) were prepared by calcining and reducing co-ion-exchanged NaY with O_2 and H_2 at 573 K, respectively. Ion-exchanged zeolites were filtered and washed with doubly distilled water until no AgCl was precipitated when $AgNO_3$ was added to filtrate. The amount of Pt and Ir exchanged were measured by atomic absorption spectrometer. Metal loadings and Ir/(Pt + Ir) ratios in the samples are summarized in Table 1. The ion-exchanged NaY's

were dried in a vacuum oven at 298 K, calcined by raising temperature from 298 to 573 K at a rate of 0.5 K/min, and kept at 573 K for 2 h in the oxygen flow of 1000 ml g^{-1} min^{-1}. Reduction was subsequently performed with H_2 (Matheson, UHP grade) at 573 K. Pt(4)/NaY and Ir(4)/NaY previously calcined and reduced were mixed with an appropriate ratio and ground in a mortar to prepare the physical mixtures of monometallic Pt and Ir clusters in N_2 atmosphere.

X-ray Diffraction

X-ray diffraction (XRD) patterns of the samples after calcination and reduction were recorded with Rigaku X-ray diffractometer using Cu$K\alpha$ radiation (Ni filtered).

^{129}Xe NMR Measurement

^{129}Xe NMR spectra were obtained at 296 K with Bruker AM 300 instrument operating at 83.0 MHz for ^{129}Xe. Each spectrum was taken after acquisition of 100 to 5000 pulse transients with a repetition time of 0.5 s. The chemical shift was referenced with respect to the chemical shift of xenon gas extrapolated to zero pressure. For ^{129}Xe NMR experiments, all the samples were pretreated in a Pyrex flow reactor which was connected to an NMR tube. The final pressure after outgassing was less than 1×10^{-5} Torr in every case. About 400 mg of sample was transferred from the reactor to the NMR tube *in situ*. The NMR tube was then sealed off with a flame. Next, 400 Torr of xenon gas (Matheson, 99.995%) was introduced into the sample tube through a vertical Pyrex stopcock at 296 K. The NMR tube containing the sample and xenon gas was then cooled in the NMR probehead to obtain low-temperature ^{129}Xe NMR spectra. The ^{129}Xe NMR spectra of physical mixtures were obtained after the physical mixtures were re-reduced with H_2 at 573 K and evacuated at 673 K for 1 h.

Hydrogen and Xenon Adsorption

The adsorption isotherms of hydrogen and xenon were obtained at 296 and 310 K, respectively, after hydrogen preadsorbed during reduction was evacuated at 673 K and 1×10^{-5} Torr for 1 h. The total number of hydrogen and xenon atoms adsorbed per metal atom was determined by extrapolating the linear portion of the isotherm to zero pressure. The sample was then evacuated at 296 K and 1×10^{-5} Torr for 1 h, and a second adsorption isotherm of hydrogen was obtained. The difference between the two adsorption isotherms extrapolated to zero pressure represents the irreversible chemisorption of hydrogen. A second adsorption isotherm of xenon was obtained from the sample preadsorbed with irreversible hydrogen.

Ethane Hydrogenolysis Reaction

Ethane hydrogenolysis reaction was carried out in a continuous-low microreactor at atmospheric pressure using helium as a diluent. H_2 (Matheson, UHP grade) and He (UHP grade) were further purified by passing through an oxytrap at room temperature followed by a molecular sieve trap. Ethane (Matheson, purity > 99.5%) was used without further purification. The experiment was carried out in the temperature range between 528 and 603 K. H_2/C_2H_6 mole ratio was 4 and the total flow rate of reactant mixture (containing 10% C_2H_6, 40% H_2, and 50% He) was 100 ml min^{-1}. The amount of sample used was 100 mg. In our experimental conditions the reaction rate was proportional to the amount of catalysts indicating the absence of external mass transfer limitations. The conversion was kept low (<5%) throughout the experiments in order to operate under differential reactor conditions. Immediately after sampling of products at 120 s on stream, ethane and H_2 were replaced with He. These experiments were repeated at various reaction temperatures to calculate the activation energy. The decrease of initial catalytic activity due to deactivation was negligible. The extent of deactivation was only about 1% of the initial activity. Products were analyzed with an on-line gas chromatograph (HP 5890A)

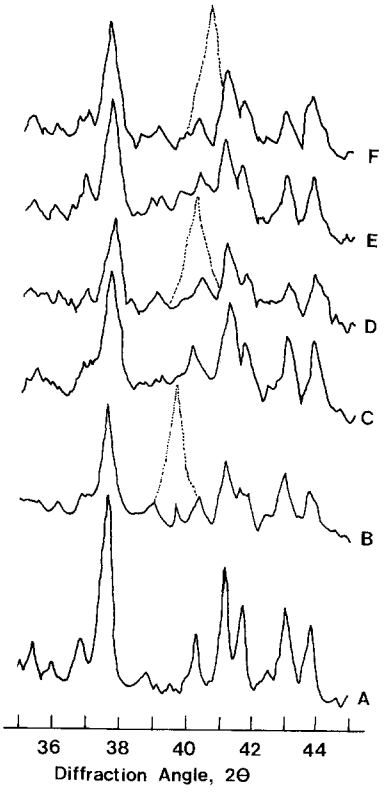

FIG. 1. X-ray diffraction patterns of NaY (A), Pt(4)/NaY (B), Pt(3)Ir(1)/NaY (C), Pt(2)Ir(2)/NaY (D), Pt(1)Ir(3)/NaY (E), and Ir(4)/NaY (F). Corresponding ion-exchanged NaY's are reduced at 573 K after calcining at 573 K (——) and 773 K (– – – –).

equipped with a 6-ft Porapak Q column and an FID detector.

RESULTS

X-ray Diffraction Study

X-ray diffraction (XRD) patterns were obtained for NaY and Pt(4)/NaY, Pt(3)Ir(1)/NaY, Pt(2)Ir(2)/NaY, Pt(1)Ir(3)/NaY, and Ir(4)/NaY prepared by calcining and reducing the corresponding ion-exchanged NaY at 573 K, respectively. The XRD patterns of Pt/NaY, Ir/NaY and Pt–Ir/NaY are almost the same as that of NaY as shown in Fig. 1, indicating that the size of the metal cluster is too small to be determined by the XRD technique. However, Pt(4)/NaY and Ir(4)/NaY prepared after calcination at 773 K and reduction at 573 K have a strong diffraction peak at the 2θ value of 39.80° and 40.64°, respectively. Pt(2)Ir(2)/NaY prepared by calcining and reducing co-ion-exchanged NaY at 773 and 573 K, respectively, have a strong peak at the 2θ value of 40.0°, which is located between the 2θ value of Pt(111) peak (39.80°) and the 2θ value of Ir(111) peak (40.64°), indicating that the metal clusters of diameter greater than 4 nm (lower limit of resolution in XRD method) were formed on the exterior surface of NaY or within the zeolite lattice if metal aggregates are occluded inside locally damaged supercages without the long-range destruction of the zeolite crystal structure.

Hydrogen and Xenon Adsorption

The results of hydrogen and xenon adsorption are shown in Table 2. The number of hydrogen atom adsorbed irreversibly per metal atom ($(H/M)_{\text{irrev.}}$) was nearly equal to unity for all the samples calcined and reduced at 573 K.

The xenon adsorption isotherms of NaY, Pt(4)/NaY, Ir(4)/NaY, Pt(2)Ir(2)/NaY, and Pt(4)/NaY preadsorbed with hydrogen (Pt(4)-H/NaY) are shown in Fig. 2. The xenon adsorption isotherms of NaY and Pt(4)-H/NaY gave a straight line with an intercept of almost zero. On the other hand, the xenon adsorption isotherms of Pt(4)/NaY, Ir(4)/NaY and Pt(2)Ir(2)/NaY showed a curvature below 50 Torr. This result can be explained by two kinds of Langmuir adsorption iso-

TABLE 2

Hydrogen and Xenon Adsorption Data

Sample	$(H/M)_{\text{irrev.}}$	Amount of Xe adsorbed[a]	No. of Xe adsorbed[b]	No. of metal atoms/cluster
Pt(4)/NaY	0.95	2.3×10^{-5}	3.8×10^{-2}	36
Pt(3)Ir(1)/NaY	0.93	2.0×10^{-5}	3.3×10^{-2}	41
Pt(2)Ir(2)/NaY	0.93	1.9×10^{-5}	3.2×10^{-2}	44
Pt(1)Ir(3)/NaY	0.97	1.9×10^{-5}	3.2×10^{-2}	44
Ir(4)/NaY	0.99	2.1×10^{-5}	3.4×10^{-2}	39

[a] mole/g-sample.
[b] atoms/supercage.

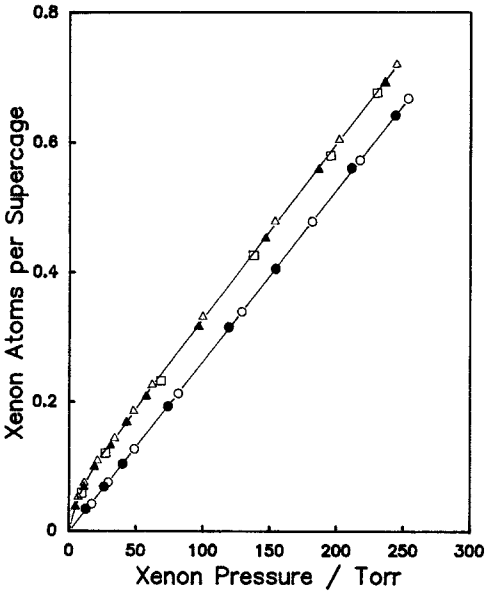

FIG. 2. The adsorption isotherms of xenon on NaY (○), Pt(4)/NaY (△), Pt(2)Ir(2)/NaY (□), Ir(4)/NaY (▲), and Pt(4)-H/NaY (●) at 310 K.

therms (*36*): one for weak adsorption on the zeolite support and the other for strong adsorption on the metal cluster. The adsorption of xenon on the metal cluster was saturated at the point where the isotherm becomes linear. An intercept obtained by the extrapolation of the linear region (50–250 Torr) of the isotherm to zero pressure will privide the amount of xenon adsorbed on the metal clusters as a monolayer when the adsorption temperature is much higher than the boiling point of xenon, as was in our case. Strong adsorption of xenon on the metal cluster did not appear in the adsorption isotherm of xenon adsorbed on Pt(4)/NaY preadsorbed with hydrogen (Pt(4)-H/NaY), as shown in Fig. 2. Thus, the chemisorbed hydrogen species do not allow a direct strong interaction of xenon with the metal cluster.

The number of xenon atoms saturated on a metal cluster will depend on the size and shape of the cluster. It has been reported that the shape of the platinum cluster in the supercage is almost spherical (*32*). The number of saturated xenon atoms will be the maximum number of xenon atoms (m) that can contact the surface of metal cluster. From the molecular models of xenon and metal cluster in the supercage, for Pt clusters consisting of 26–55 atoms in the supercage, m may be assumed to be 4 because only one xenon atom of 0.43 nm size can be in contact with the cluster through a supercage aperture of 0.74 nm in diameter. For a Pt cluster smaller than this size range, xenon will be able to enter the supercage containing the cluster, and therefore m will become greater than 4. The m-values thus obtained are approximately 7 for the cluster of 13 Pt atoms, 6 for the cluster of 17 Pt atoms, and 5 for the cluster of 19 Pt atoms. With the result of xenon adsorption, the average number of metal atom per cluster (N) can be obtained as

$$N = m\,M/X,$$

where M is the total number of metal atoms in the sample and X is the number of xenon atoms adsorbed on metal cluster corresponding to the strong adsorption on the metal clusters in the sample. Previous studies (*32, 33*) and our TEM study (*37*) indicated that Pt clusters in NaY are almost monodisperse and that the average diameter of Pt clusters is about 1 nm. The value of N thus-obtained can check the assumption used for m. Using successive iteration with a new value of m until N and m are in agreement, one can obtain the value of N in a self-consistent manner. For example, the amount of strong xenon adsorption on Pt(4)/NaY was $2.3\ (+0.1) \times 10^{-5}$ mole per g-sample (corresponding to $3.8\ (+0.2) \times 10^{-2}$ Xe atoms per supercage for X as shown in Table 2). The M value of Pt(4)/NaY is 0.34 Pt atoms per supercage (2.7 Pt atoms per unit cell of zeolite Y). Starting with the assumption that the average number of Pt atom per cluster (N) is close to 17, the m-value is 6 Xe atoms per cluster, as mentioned above. Then, we can obtain $N = \mathrm{m\ M/X} = 6 \times 0.34/(3.8 \times 10^{-2}) = 54$ Pt atoms per cluster. This result is not consistent with

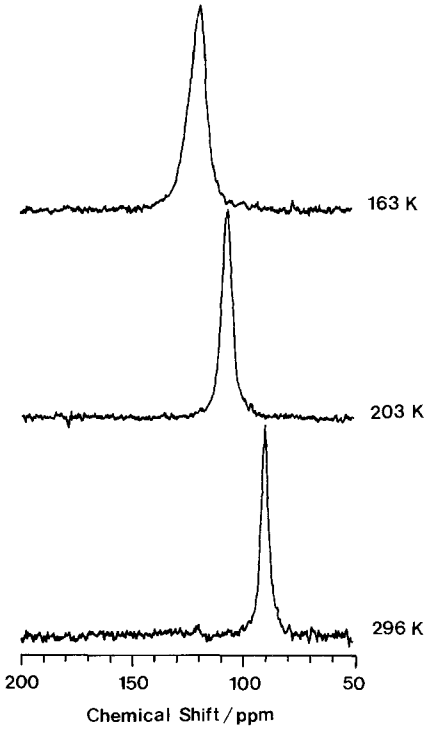

FIG. 3. Low-temperature ^{129}Xe NMR spectra of bimetallic Pt(2)Ir(2)/NaY catalyst under 400 Torr of xenon at 296 K.

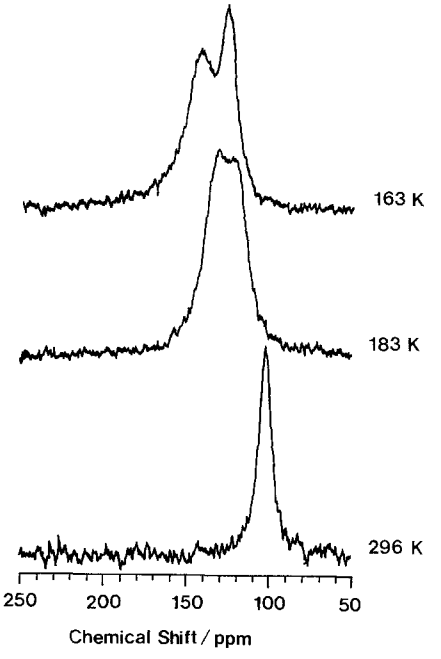

FIG. 4. Low-temperature ^{129}Xe NMR spectra obtained from 1 : 1 physical mixture of Pt(4)NaY and Ir(4)/NaY under 400 Torr of xenon at 296 K.

the assumption of 6 for m. With another m value of 4, we can obtain $N = 36$ Pt atoms per cluster, which is consistent with $m = 4$. The numbers of metal atoms per cluster obtained by this method are summarized in Table 2. This assessment showed that the metal clusters contain about 40 atoms in all the samples containing 4 wt% of total metal loading of Pt and Ir.

^{129}Xe NMR Data

Figures 3, 4, and 5 show the low-temperature ^{129}Xe NMR spectra of Pt(2)Ir(2)/NaY, 1 : 1 physical mixture and 3 : 1 physical mixture of Pt(4)/NaY and Ir(4)/NaY, respectively. The ^{129}Xe NMR spectra of bimetallic Pt(2)Ir(2)/NaY catalyst show only one NMR peak with decreasing NMR recording temperature. However, physical mixture samples have two ^{129}Xe NMR peaks arising from Pt(4)/NaY and Ir(4)/NaY. Figure 6 shows

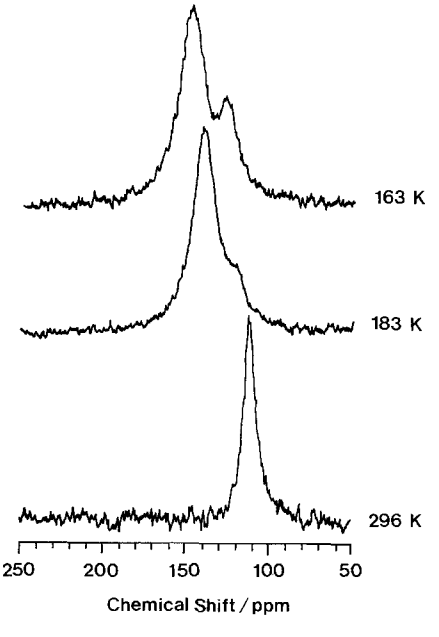

FIG. 5. Low-temperature ^{129}Xe NMR spectra obtained from 3 : 1 physical mixture of Pt(4)NaY and Ir(4)/NaY under 400 Torr of xenon at 296 K.

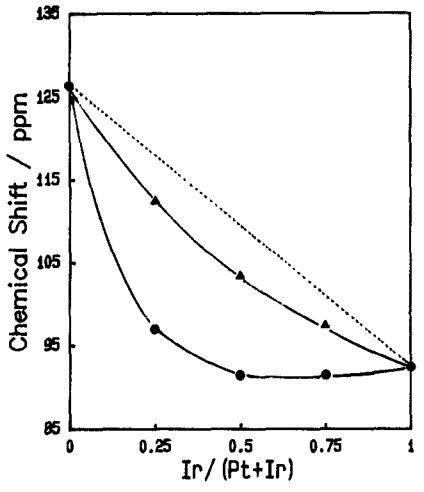

FIG. 6. The ^{129}Xe NMR chemical shifts of the physical mixtures of Pt(4)/NaY and Ir(4)/NaY (▲) and bimetallic catalysts containing 4 wt% of total metal loading (●) as a function of Ir/(Pt + Ir).

correlation between Ir content (Ir/(Pt + Ir)) and the ^{129}Xe NMR chemical shifts of Pt(4)/NaY, Ir(4)/NaY, the physical mixtures of Pt(4)/NaY and Ir(4)/NaY, and a series of bimetallic Pt–Ir/NaY. The chemical shift of Pt(4)/NaY (Ir/(Pt + Ir) = 0), 126.4 ppm, is much larger than that of Ir(4)/NaY (Ir/(Pt + Ir) = 1), 92.5 ppm. The chemical shifts of Pt–Ir/NaY decrease with increasing the ratio of Ir/(Ir + Pt) to 0.5. However, the chemical shifts of Pt–Ir/NaY containing Ir more than 50 mole% do not change very much. The chemical shifts of Pt(2)Ir(2)/NaY (Ir/(Pt + Ir) = 0.50) and Pt(1)Ir(3)/NaY (Ir/Pt + Ir) = 0.75) are slightly smaller than that of monometallic Ir(4)/NaY (Ir/(Pt + Ir) = 1). The chemical shifts of physical mixtures decrease with increasing the Ir/(Pt + Ir) ratio. This pattern in the chemical shifts of physical mixtures is different from that of bimetallic Pt–Ir/NaY and similar to that of ideal physical mixture, which should be a diagonal line connecting the chemical shift of Pt(4)/NaY and Ir(4)/NaY.

Ethane Hydrogenolysis Reaction

The reaction temperature was chosen at 558 K such that Pt(4)/NaY catalyst is not active and the deactivation due to the formation of coke is negligible. Turnover frequency (TOF) was calculated by the expression

$$\text{TOF} = C/W,$$

where C is the number of ethane molecules reacted per unit time and W is the number of surface metal sites measured by the hydrogen chemisorption as shown in Table 2.

As the Ir/(Pt + Ir) ratio increases, the TOFs of bimetallic clusters containing 4 wt% of total metal loading of Pt and Ir and physical mixture samples of Pt(4)/NaY and Ir(4)/NaY increase in a different manner, as shown in Fig. 7. The TOFs of physical mixture catalysts are always greater than those of bimetallic Pt–Ir/NaY catalysts containing the corresponding amounts of Pt and Ir. The influence of temperature on the activity of the catalysts was studied in the temperature range between 528 and 603 K. The Arrhenius plots for all the catalysts give straight lines, as shown in Fig. 8. The activation energies are listed in Table 3. The activation energies of Pt–Ir/NaY bimetallic clusters are smaller than those of monometallic Pt(4)/NaY and Ir(4)/NaY clusters.

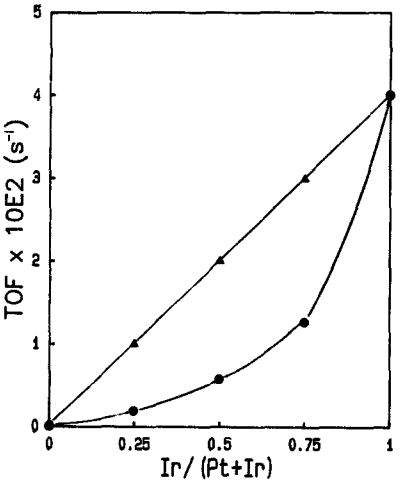

FIG. 7. TOFs of the physical mixtures of Pt(4)/NaY and Ir(4)/NaY (▲) and bimetallic catalysts containing 4 wt% of total metal loading (●) as a function of Ir/(Pt + Ir) in ethane hydrogenolysis at 558 K.

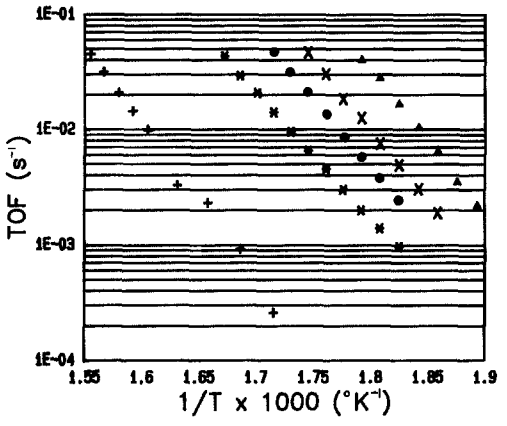

FIG. 8. Arrhenius plot of ethane hydrogenolysis catalyzed over Pt(4)/NaY (+), Pt(3)Ir(1)/NaY (*), Pt(2)Ir(2)/NaY (●), Pt(1)Ir(3)/NaY (×), and Ir(4)/NaY (▲).

DISCUSSION

If we can assume that adsorption stoichiometry between H and metal atoms is 1, $(H/M)_{irrev.}$ ratios observed are consistent with clusters of about 1 nm in diameter, which is in agreement with xenon adsorption results (Table 2). The TEM micrographs of the samples calcined and reduced at 573 K revealed the formation of about 1-nm clusters inside the zeolite crystallites (*37*). Sachtler and co-workers (*38, 39*) reported that platinum clusters prepared after calcining and reducing Pt ion-exchanged NaY at 573 K were located in the zeolite supercage. Almost the same amounts of xenon adsorbed on the metal clusters indicate that the approximately same number and size of metal clusters were formed inside the zeolite supercage of our samples. Therefore, the chemical shifts in the ^{129}Xe NMR spectra of the samples containing 4 wt% total metal loading of Ir and Pt are mostly attributed to the nature of metal cluster itself.

TABLE 3

Activation Energy of Ethane Hydrogenolysis Reaction

Catalyst	Activation energy (KJ/mol)
Pt(4)/NaY	257.5 ± 4.2
Pt(3)Ir(1)/NaY	210.4 ± 1.7
Pt(2)Ir(2)/NaY	226.8 ± 2.1
Pt(1)Ir(3)/NaY	234.4 ± 2.5
Ir(4)/NaY	245.3 ± 2.9

The 1 : 1 and 3 : 1 physical mixture of Pt(4)/NaY and Ir(4)/NaY have only one NMR peak at 296 K, as shown in Figs. 4 and 5. However, two NMR peaks attributed to monometallic Pt and Ir clusters appeared at 163 K. The NMR peaks at 144.0 and 126.4 ppm in Fig. 4 are originated from Pt clusters in Pt(4)/NaY and Ir clusters in Ir(4)/NaY, respectively. Similarly, the NMR peaks at 146.3 ppm and 127.2 ppm in Fig. 5 are also attributed to Pt and Ir clusters, respectively. The difference of 2.3 ppm in the chemical shifts between Pt clusters in two physical mixture samples is believed due to the difference of xenon concentration in each sample as the sample cell was cooled into the NMR probe head, because the amount of samples is slightly different inside NMR cell due to the difficulty of *in situ* transferring powder samples completely to the NMR cell. The observation of two NMR bands at low temperature is consistent with the results of Ryoo *et al.* (*40*) and Yang *et al.* (*41*), indicating that the exchange of xenon between separated Pt and Ir cluster is not fast enough to show only a single averaged ^{129}Xe NMR signal at 163 K. The distance between the crystallites of physical mixture becomes longer than the flight distance of the xenon during the NMR measurement time at 163 K because of the lower diffusivity of xenon atom. However, the ^{129}Xe NMR spectrum of bimetallic Pt(2)Ir(2)/NaY shows only one peak at 163 K. This suggests that Pt(2)Ir(2)/NaY consists of Pt–Ir bimetallic clusters or consists of monometallic Pt and Ir clusters closely separated which cannot be distinguished by ^{129}Xe NMR at 163 K. According to the result of de Menorval *et al.* (*28*) the chemical shift of ^{129}Xe adsorbed on Y zeolite increased linearly with the number of ions on which xenon

atoms adsorb. The approximately same size and number of metal clusters are present inside the zeolite supercages of Pt(4)/NaY, Ir(4)/NaY, and Pt–Ir/NaY, as shown in Table 2. Therefore, if bimetallic Pt–Ir/NaY clusters consist of monometallic Pt and Ir clusters closely separated, the chemical shifts of Pt–Ir/NaY bimetallic catalysts should follow the average chemical shift calculated from the chemical shifts of monometallic Pt and Ir clusters, represented as a dotted line in Fig. 6. However, the chemical shifts of Pt–Ir/NaY bimetallic sample are considerably lower than those of physical mixture samples. These results indicate that surface Pt atoms are replaced with Ir atoms which has a chemical shift lower than Pt to form a bimetallic cluster of Pt and Ir. The change in the electron band structure due to the formation of bimetallic cluster might cause the xenon atoms adsorbed on bimetallic clusters to be polarized less than xenon atoms adsorbed on Pt clusters, resulting in the lower chemical shifts of bimetallic clusters.

The chemical shifts of physical mixtures are deviated from a dotted line in Fig. 6. The surface area of the physical mixture becomes larger than that of Pt(4)/NaY or Ir(4)/NaY arising from the formation of new external surface by crushing. Therefore, the number of supercage itself and clusters inside the supercage decrease, resulting in the chemical shifts of physical mixture samples lower than the weight-averaged chemical shift of Pt(4)/NaY and Ir(4)/NaY, because the metal clusters on the exterior surface of the zeolite contribute to polarizing xenon atoms much less than those inside the zeolite structure.

Ethane hydrogenolysis reaction requires the active sites comprising of adjacent metal atom ensemble. If the catalytically active Ir atoms are diluted with inactive Pt atoms, the probability of forming an active Ir ensemble will decline sharply. This is the concept of the geometric effect. Another concept, electronic effect, is based on the assumption that the nature and strength of a chemical bond between an adsorbate atom and a surface atom are influenced by the neighbors of the surface atom. This electronic effect was partially realized in the nonlinear decrease of chemical shift of ^{129}Xe NMR as discussed above. The TOFs of physical mixture catalysts linearly increase with the content of Ir. However, TOFs of bimetallic Pt–Ir/NaY catalysts are lower by 2.5–5 times than those of corresponding physical mixture catalysts. As can be seen in Fig. 7, the addition of Pt leads to a significant decrease in the activity of Pt–Ir bimetallic catalysts. TOFs of Pt(2)Ir(2)/NaY and Pt(1)Ir(3)/NaY are greater by about 2.5 and 6.5 times than that of Pt(3)Ir(1)/NaY, respectively. These results can be explained by the geometric effect of Pt–Ir bimetallic cluster such that the probabilities of finding Ir atom as a neighbor of Ir atom are about 6, 24, and 56% in Pt(3)Ir(1)/NaY, Pt(2)Ir(2)/NaY, and Pt(1)Ir(3)/NaY, respectively. Activation energy data show that new, more active sites are more preferentially exhibited when Pt is added to Ir. Also, the TOF plot shows Pt preferentially covers the surface. These are consistent with the idea that as Pt is covering the flat surface, what is left are the more active Ir corners and edges. However, this kind of covering effect of Pt is not observed in the physical mixture catalysts as expected. Smale and King (*42*) reported that bimetallic Ru–Cu/SiO_2 catalysts have different activation energies in the ethane hydrogenolysis reaction. They interpreted the changes in activation energy as an electronic effect of Cu on Ru. The activation energies of Pt–Ir/NaY bimetallic catalysts are smaller than those of monometallic Pt(4)/NaY and Ir(4)/NaY, which suggests the existence of electronic interaction due to the formation of Pt–Ir bimetallic clusters.

CONCLUSIONS

Hydrogen and xenon adsorption and XRD results indicated that very small (about 1 nm in diameter) metal clusters of approximately the same size were formed inside the zeolite supercage for Pt(4)/NaY, Ir(4)/NaY,

and a series of Pt–Ir/NaY bimetallic catalysts containing 4 wt% of total metal loading of Pt and Ir after calcining and reducing at 573 K. Low-temperature ^{129}Xe NMR spectra of bimetallic Pt(2)Ir(2)/NaY showed only one NMR peak, while the NMR spectra of the physical mixtures of Pt(4)/NaY and Ir(4)/NaY showed two ^{129}Xe NMR peaks originated from separated monometallic Pt and Ir clusters at 163 K, respectively. The chemical shifts in ^{129}Xe NMR spectroscopy and catalytic activities in ethane hydrogenolysis reaction (TOFs) of Pt–Ir/NaY bimetallic samples were lower than those of corresponding physical mixtures of Pt(4)/NaY and Ir(4)/NaY. With increasing the Ir content in Pt–Ir/NaY samples, the chemical shifts decreased and the catalytic activities (TOFs) increased, which resulted from the coverage of surface Pt atom by Ir atom. The activation energies of Pt–Ir/NaY catalysts were smaller than those of Pt(4)/NaY and Ir(4)/NaY catalyst and the TOFs of bimetalic Pt–Ir catalysts are much smaller than those of the physical mixture containing the corresponding amounts of Pt and Ir, which indicates the existence of electronic interaction between Pt and Ir in Pt–Ir/NaY.

ACKNOWLEDGMENT

This research was funded by the Korea Science and Engineering Fund (1990–1993).

REFERENCES

1. Sinfelt, J. H., U.S. Patent No. 3953368 (1976).
2. Ramaswamy, A. V., Ratnasamy, P., and Sivasanker, S., *in* "Proceedings, 6th International Congress on Catalysis, London, 1976" (G. C. Bond, P. B. Wells, and F. C. Tompkins, Eds.), Vol. 2, p. 855. The Chemical Society, London, 1977.
3. Rasser, J. C., Beindorff, W. H., and Scholten, J. J. F., *J. Catal.* **59,** 211 (1979).
4. Rice, R. W., and Lu, K., *J. Catal.* **77,** 104 (1982).
5. Charcosset, H., *Rev. Inst. Fr. Pet.* **34,** 238 (1979).
6. Kluksdahl, H. E., U.S. Patent No. 3415737 (1968).
7. Biloen, P., Helle, J. N., Verbeek, H., Dautzenberg, F. M., and Sachtler, W. M. H., *J. Catal.* **63,** 112 (1980).
8. Shum, V. K., Butt, J. B., and Sachtler, W. M. H., *J. Catal.* **99,** 126 (1986).
9. Dautzenberg, F. M., Helle, J. N., Biloen, P., and Sachtler, W. M. H., *J. Catal.* **63,** 119 (1988).
10. Burch, R., and Garla, L. C., *J. Catal.* **71,** 360 (1981).
11. Haensel, V., U.S. Patent No. 2479109 (1949).
12. Haensel, V. U.S. Patent No. 2479110 (1949).
13. Dalla Betta, R. A., and Boudart, M., *in* "Proceedings, 5th International Congress on Catalysis, Palm Beach, 1972" (J. W. Hightower, Ed.), Vol. 2, p. 1329. North-Holland, Amsterdam, 1973.
14. Gallezot, P., *Catal. Rev.-Sci. Eng.* **20,** 21 (1979).
15. Elliott, D. J., and Lunsford, J. H., *J. Catal.* **57,** 11 (1979).
16. Tebassi, L., Sayari, A., Ghorbel, A., Dufaux, M., and Naccache, C., *J. Mol. Catal.* **25,** 397 (1984).
17. Tri, T. M., Massardier, J., Gallezot, P., and Imelik, B., *J. Catal.* **85,** 244 (1984).
18. Augustine, S. M., Nacheff, M. S., Tsang, C. M., Butt, J. B., and Sachtler, W. M. H., *In* "Catalysis 1987" (J. W. Ward, Ed.), p. 1. Elsevier, Amsterdam, 1988.
19. Moretti, G., and Sachtler, W. M. H., *J. Catal.* **115,** 205 (1987).
20. Chan, I. Y., Csencsits, R., O'Keefe, M. A., and Gronsky, R., *J. Catal.* **103,** 466 (1987).
21. Shastri, A. G., Schwank, J., and Galvagno, S., *J. Catal.* **100,** 446 (1986).
22. Sinfelt, J. H., Via, G. H., and Lytle, F. W., *J. Chem. Phys.* **72,** 4832 (1980).
23. Sinfelt, J. H. Via, G. H., Lytle, F. W., and Greegor, R. B., *J. Chem. Phys.* **75,** 5527 (1981).
24. Sinfelt, J. H., Via, G. H., and Lytle, F. W., *J. Chem. Phys.* **76,** 2779 (1982).
25. Tzou, M. S., Teo, B. K., and Sachtler, W. M. H., *Langmuir* **2,** 773 (1986).
26. Garten, R. L., and Sinfelt, J. H., *J. Catal.* **62,** 127 (1980).
27. Lazar, K., Reiff, W. M., Morke, W., and Guczi, L., *J. Catal.* **100,** 118 (1986).
28. de Menorval, L. C., Fraissard, J. P., and Ito, T., *J. Chem. Soc. Faraday Trans. 1* **78,** 403 (1982).
29. Ito, T, de Menorval, L. C., and Fraissard, J. P., *J. Chim. Phys.* **80,** 573 (1983).
30. Ito, T., de Menorval, L. C., Guerrier, E., and Fraissard, J. P., *Chem. Phys. Lett.* **111,** 271 (1984).
31. Scharpf, E. W., Crecely, R. W., Gates, B. C., and Dybowski, C., *J. Phys. Chem.* **90,** 9 (1986).
32. Boudart, M., Samant, M. G., and Ryoo, R., *Ultramicroscopy* **20,** 125 (1986).
33. Chmelka, B. F., Ryoo, R., Liu, S.-B., de Menorval, L. C., Radke, C. J., Petersen, E. E., and Pines, A., *J. Am. Chem. Soc.* **110,** 4468 (1988).
34. Forger, K., and Jaeger, H., *J. Catal.* **70,** 53 (1981).
35. Kuijers, F. J., and Ponec, V., *Appl. Surf. Sci.* **2,** 43 (1978).

36. Ryoo, R., Cho S. J., Pak, C., Kim, J. G., Ihm, S. K., and Lee, J. Y., *J. Am. Chem. Soc.* **114,** 76, (1992).
37. Yang, O. B., Lee, J. Y., Ryoo, R., and Woo S. I., in preparation (1991).
38. Tzou, M. S., and Sachtler, W. M. H., *in* "Catalysis 1987" (J. W. Ward, Ed.), p. 233. Elsevier, Amsterdam, 1988.
39. Tzou, M. S., Teo, B. K., and Sachtler, W. M. H., *J. Catal.* **113,** 220 (1988).
40. Ryoo, R., Pak, C., Lee, H. W., and Chmelka, B. F., *Zeolites* **10,** 790 (1990).
41. Yang, O. B., Woo, S. I., and Ryoo, R., *J. Catal.* **123,** 375 (1990).
42. Smale, M. W., and King, T. S., *J. Catal.* **119,** 441 (1989).